1.Classification *INPE-COM.10/PE* *CDU:621.372.832.8*	2.Period *December, 1975*	4.Distribution Criterion internal ☐ external [X]
3.Key Words (selected by the author) *DISK, NETWORK*		
5.Report No. *INPE-927-PE/035*	6.Date *August, 1976*	7.Revised by *Pawel Rozenfeld*
8. Title and Sub-title *ANALYSIS OF DISK NETWORKS ON MAGNETIC SUBSTRATE*		9.Authorized by *Nelson de Jesus Parada* *Director*
10.Sector *CET*	Code *403*	11.No. of Copies 15
12.Authorship *René R. Bonetti and Plinio Tissi* 13.Signature of first author		14.No. of Pages - *33* 15.Price

16.Summary/Notes

The impedance matrix of a disk n-port on magnetic substrate is determined, fringing fields at the disk edge being included in the analysis. The theory lends itself well to computational implementation and numerical design, which is demonstrated with the synthesis of a 4-port circulator. Classical results for the 3-port circulator are verified. Experimental evidence is presented through the construction of a broadband 4-port circulator.

17.Remarks *To be submitted for publication in IEEE Trans. on Microwave Theory and Techniques.*

NOMENCLATURE

μ, κ	diagonal and off-diagonal elements of the Polder tensor [12]
κ/μ	gyrotropy
ϵ_i, μ_i	permittivity and effective permeability of region i (i = 1,2)
Y_e	intrinsic wave admittance of region 1
β_i, k_i	depth and radial wave-numbers
Ω	normalized frequency
r, ϕ, z	cylindrical coordinates
R_1, R_2	disk and cavity radii
K	number of ports
γ_i, Γ_i	sectors of disk edge
h	magnetic substrate thickness
t	disk conductor thickness
$2\psi_i$	coupling angle at i-th port
J_n, Y_n	Bessel functions of first and second kind and order n
I_n, K_n	special Bessel functions of first and second kind
$\sum_n$	summation over all integers
$\sum_m$	summation over all non-negative integers, unless otherwise specified
$\tilde{R}_1$, $\tilde{R}_2, \tilde{t}$	normalized quantities, with respect to h
H_i	tangential magnetic field component at i-th port

ANALYSIS OF DISK NETWORKS ON MAGNETIC SUBSTRATE

Renē Roberto Bonetti and Plinio Tissi

ABSTRACT - The impedance matrix of a disk n-port on magnetic substrate is determined, fringing fields at the disk edge being included in the analysis. The theory lends itself well to computational implementation and numerical design, which is demonstrated for the synthesis of 4-port circulators. Classical results for the 3-port circulator are verified. Experimental evidence is presented through the construction of a broadband 4-port circulator.

I. INTRODUCTION

Planar network theory is becoming a powerful tool for the design of microwave integrated circuits. When compared to other physical structures, planar networks offer the designer considerable freedom, due not only to their size and shape, but also to the large variety of devices realizable from simple geometries.

A very simple shape, the disk, has already proven very useful for the realization of junction circulators and presents interesting possibilities for other devices.

The existing theories for planar networks [1] - [7] in general, do not

---

The authors are with the Instituto de Pesquisas Espaciais, São José dos Campos, São Paulo, Brazil.

include the fringing fields in the analysis, with consequent limitations on the frequency and power ranges of their applicability to numerical design techniques. With respect to this problem we quote Bosma [10]: "It is the unsolved problem of the fringing field that makes numerical design of circulators not yet very spectacular".

This paper presents a theory for the shielded disk n-port, which includes fringing fields, and is therefore appropriate for the design of classical as well as edge-guided wave circulators. The theory lends itself well to computational implementation and numerical synthesis since the eigenfunctions are computed independently of the number, positions and widths of the ports. Consequently, the search for optimum port parameters is performed by means of relatively simple algorithms.

II. FORMULATION OF GEOMETRY AND BASIC HYPOTHESES

The planar network consists of a highly conducting disk placed between two disk-shaped magnetic substrates (Fig. 2), and coupled to K ports, arranged along its periphery in such a way that no two ports have any points in common (Fig. 3). The whole is confined within a concentric cylindrical cavity with perfectly conducting walls (Fig. 1). The magnetization is in the z-direction and is restricted to the region of the disk.

The ports are assumed to be coupled to TEM-mode striplines, each spanning an angle $2\psi_i$ ($i = 1, 2, \ldots, K$) at the edge of the disk. The sector coupled to the i-th line is denoted by γ_i. The angular position of the center of the i-th port relative to port # 1, is σ_i. Due to the TEM-mode excitation only disk modes with r.f. magnetic fields parallel to the ground plates need be considered. Assuming that the operating frequency range is given by

$$f < 1/\left[2h(\mu_1\varepsilon_1)^{1/2} \right] \tag{1}$$

the z-independent modes are dominant in the magnetized region (see Appendix).

III. FORMAL SOLUTION OF THE FIELD PROBLEM

The general expression for the z-independent modes in the magnetized region are the well known expansions [1]:

$$E_z^{(1)}(r,\phi) = \sum_n M_n J_n(k_1 r)\, e^{-jn\phi} \tag{2}$$

$$H_\phi^{(1)}(r,\phi) = -j\, Y_e \sum_n M_n F_n(k_1 r, \kappa/\mu)\, e^{-jn\phi} \tag{3}$$

$$H_r^{(1)}(r,\phi) = Y_e \sum_n M_n \left[\frac{nJ_n(k_1 r)}{k_1 r} - \frac{\kappa}{\mu} J_n'(k_1 r) \right] e^{-jn\phi} \tag{4}$$

where

$$F_n(k_1 r, \kappa/\mu) = J_n'(k_1 r) - \frac{\kappa}{\mu} \cdot \frac{nJ_n(k_1 r)}{k_1 r}$$

and $0 \leq z \leq h$. In the region $h + t \leq z \leq 2h + t$, the fields are obtained by symmetry. Time dependence $e^{j\omega t}$ is understood.

The main steps in the derivation of the eigenfunctions for the outer fields are given in the Appendix. In terms of those functions, the fields between consecutive strips can be writen as[1]

---

[1] *In order to write general expressions for the fields below and above cut-off the symbol* C_n' *here means derivative with respect to the variable* r. *For simplicity,* k_2 *and* β_2 *stand for* k_{2m} *and* β_{2m}, *respectively.*

$$E_z^{(2)}(r,\phi,z) = \sum_n \sum_m A_{nm}\, C_n(k_2 r)\, \cos\beta_2 z \,.\, e^{-jn\phi} \tag{5.a}$$

$$E_r^{(2)}(r,\phi,z) = -\sum_n \sum_m A_{nm}\, \beta_2\, k_2^{-2}\, C_n'(k_2 r)\, \sin\beta_2 z.e^{-jn\phi} \tag{5.b}$$

$$E_\phi^{(2)}(r,\phi,z) = j \sum_n \sum_m A_{nm}\, \beta_2\, (k_2^2 r)^{-1}\, C_n(k_2 r)\, \sin\beta_2 z.ne^{-jn\phi} \tag{5.c}$$

$$H_r^{(2)}(r,\phi,z) = \omega\varepsilon_2 \sum_n \sum_m A_{nm}\, (k_2^2 r)^{-1}\, C_n(k_2 r)\, \cos\beta_2 z.ne^{-jn\phi} \tag{5.d}$$

$$H_\phi^{(2)}(r,\phi,z) = -j\omega\varepsilon_2 \sum_n \sum_m A_{nm}\, k_2^{-2}\, C_n'(k_2 r)\, \cos\beta_2 z.e^{-jn\phi} \tag{5.e}$$

where

$$C_n(k_2 r) = \begin{cases} J_n(k_2 r) - \dfrac{J_n(k_2 R)}{Y_n(k_2 R)}\, Y_n(k_2 r) & \text{for } \omega(\mu_2\varepsilon_2)^{1/2} > \beta_2 \\ K_n(jk_2 r) - \dfrac{K_n(jk_2 R)}{I_n(jk_2 R)}\, I_n(jk_2 r) & \text{for } \omega(\mu_2\varepsilon_2)^{1/2} < \beta_2 \end{cases}$$

and the expansions are valid in the whole interval $0 \leq z \leq 2h + t$.

In the regions below and above the striplines the fields will be assumed to be those of pure TEM-modes as in previous works [1], [2].

The fringing fields described by (5) will, of course, be perturbed in the neighborhood of the coupling lines, however this effect is negligible below cut-off, which is the case of most actual devices. The eigenfunctions necessary for operation above cut-off were introduced for completeness.

The relationship between the two sets of mode coefficients, M_n and A_{nm} is obtained from the continuity of E_z at the edge of the disk:

$$E_z^{(1)}(R_1,\phi) = E_z^{(2)}(R_1,\phi, z) \tag{6}$$

in $0 < z < 2h + t$, $\phi \in \Gamma_i$ $(i = 1, 2, \ldots, K)$.

The symmetry of the structure allows the inner field to be expanded in a Fourier series in the z variable (See Fig. 4) as

$$E_z^{(1)}(R_1,\phi) = 2E_o(\phi) \sum_m \frac{(1-\cos m\pi)}{m\pi} \sin\left(\frac{m\pi}{2h+t}h\right)\cos\left(\frac{m\pi}{2h+t}z\right) \tag{7}$$

where

$$E_o(\phi) = \sum_n M_n J_n(k_1R_1)\, e^{-jn\phi} \tag{8}$$

The boundary condition (6) permits the identification of expansions (5.a) and (7), which yields

$$A_{nm} = 0 \qquad m \text{ even} \tag{9.a}$$

$$A_{nm} = \frac{4}{m\pi} \sin\left(\frac{m\pi h}{2h+t}\right) \frac{J_n(k_1R_1)}{C_n(k_1R_1)} M_n \qquad m \text{ odd} \tag{9.b}$$

Equations (9) show how the outer fields in the sectors Γ_i, are completely determined by the inner fields.

The continuity of the tangential magnetic field component on the disk edge provides the relationship between the coefficients M_n and the port excitations.

We have

$$H_\phi^{(1)}(R_1,\phi) + (\text{higher order depth modes}) = H_\phi^{(2)}(R_1,\phi,z) \tag{10}$$

for $0 \leq z \leq h$ and $\phi \in \Gamma_i$.

The integration of (10) along the disk depth yields

$$H_\phi^{(1)}(R_1,\phi) = \frac{1}{h}\int_0^h H_\phi^{(2)}(R_1,\phi,z)\, dz \tag{11}$$

since the contribution of the higher order depth modes, which vary as $\cos(m\pi z/h)$ (See Appendix) is nihil.

The integration is performed using the expansion (5.e) by eliminating the coefficients A_{nm} through (9). The result is

$$H_\phi^{(1)}(R_1,\phi) = -2j\omega\varepsilon_2\, R_1 \sum_n M_n J_n(k_1 R_1)\, \Lambda_n\, e^{-jn\phi} \tag{12}$$

in which we define the fringing function of order n as

$$\Lambda_n \equiv \Lambda_n\,(\Omega,\ \bar{R}_1,\ \bar{R}_2,\ \bar{t}) = \frac{2}{2+\bar{t}} \sum_{m=1,3..}^{\infty} \left(\frac{\sin\beta_2 h}{\beta_2 h}\right)^2 \frac{1}{\chi^2}\,\frac{C_n'(\chi)}{C_n(\chi)} \tag{13}$$

with

$$\Omega = \omega h(\mu_2\varepsilon_2)^{1/2}$$

$$\chi^2 = k_2^2 R_1^2 = \left[\ \Omega^2 - \left(\frac{m\pi}{2+\bar{t}}\right)^2\ \right] \bar{R}_1^2$$

We point out that the tangential magnetic field component is given by (12) only in the sectors Γ_i and is defined at the inner end of the lines, on γ_i, by the port excitation H_i. The inversion of expansion (3) yields

$$M_p = j(2\pi Y_e F_p)^{-1} \sum_{i=1}^{K} \left[\int_{\gamma_i} H_i \, e^{jp\phi} \, d\phi + \int_{\Gamma_i} H_\phi^{(1)}(R_1,\phi) \, e^{jp\phi} \, d\phi \right] \tag{14}$$

$p = 0, \pm 1, \pm 2, \ldots$

Substituting (12) in this equation and defining

$$b_{pi} = \int_{-\psi_i}^{\psi_i} \exp\left[jp(\phi+\sigma_i)\right] \, d\phi \tag{15}$$

$$T_{np} = \sum_{i=1}^{K} \int_{\Gamma_i} \exp\left[j(p-n)\phi\right] \, d\phi \tag{16}$$

we obtain

$$F_p M_p - \frac{k_1 R_1}{\pi} \frac{\varepsilon_2}{\varepsilon_1} \sum_n \Lambda_n M_n T_{np} J_n(k_1 R_1) = \frac{j}{2\pi Y_e} \sum_{i=1}^{K} H_i \, b_{pi} \tag{17}$$

$p = 0, \pm 1, \pm 2, \ldots$

This set of equations, together with (9), completely solves the field problem for a TEM-coupled disk on a general magnetic substrate when the fringing fields are taken into account.

IV. NATURAL FREQUENCIES

In the uncoupled case, $\psi_i = 0$ $(i = 1, 2, \ldots, K)$, hence

$$T_{np} = \begin{cases} 0 & p \neq n \\ 2\pi & p = n \end{cases}$$

$$b_{pi} = 0 \quad \text{all } p, i \ .$$

Equation (17) then yields:

$$M_n \left[F_n(k_1 R_1, \kappa/\mu) - 2k_1 R_1 (\varepsilon_2/\varepsilon_1) \Lambda_n (\Omega, \bar{R}_1, \bar{R}_2, \bar{t}) J_n(k_1 R_1) \right] = 0 \qquad (18)$$

$n = 0, \pm 1, \pm 2, \ldots$

If the ratio R_1/h is such that the fringing function is negligible (see Fig. 5), then the resonance condition coincides, as expected, with the classical one [1].

$$J_n'(k_1 R_1) - \frac{\kappa}{\mu} \cdot \frac{n J_n(k_1 R_1)}{k_1 R_1} = 0 \qquad (19)$$

Let $(\kappa/\mu)_{on}$ be the unperturbed value of the gyrotropy at resonance of mode n, found as a root of (19). From (18) we find that the effect of the fringing fields will be to shift this value to

$$(\kappa/\mu)_n = (\kappa/\mu)_{on} - \frac{2(k_1 R_1)^2 \varepsilon_2}{n \varepsilon_1} \Lambda_n \qquad (20)$$

When the exterior modes are below cut-off the fringing function is positive (Figs. 5, 6), therefore the resonances of the positive modes ($n > 0$) will be shifted to lower values of girotropy and the negative ones to higher values (Fig. 7). The isotropic resonances of the degenerate modes will then be shifted to lower frequencies, which is in agreement with the results found in [9] for the particular case of $\bar{R}_2 = \infty$, $\bar{t} = 0$, $\varepsilon_2 = \varepsilon_1$, $\kappa/\mu = 0$.

V. IMPEDANCE MATRIX

In this section a relationship between the port voltages and currents at the disk reference planes is first derived followed by the determination of the impedance matrix of the K-port.

To this end we introduce the following matrices

$$\underset{\sim}{m} = [M_{-N}\ M_{-N+1} \cdots M_N]^t$$

$$\underset{\sim}{\xi} = [H_1\ H_2 \cdots H_K]^t$$

$$\underset{\sim}{v} = [V_1\ V_2 \cdots V_K]^t$$

$$\underset{\sim}{i} = [I_1\ I_2 \cdots I_K]^t$$

$$\underset{\approx}{\Lambda} = \text{diag}\,[\Lambda_{-N}, \Lambda_{-N+1} \cdots \Lambda_N]$$

$$\underset{\approx}{F} = \text{diag}\,[F_{-N}, F_{-N+1} \cdots F_N]$$

$$\underset{\approx}{J} = \text{diag}\,|J_{-N},\ J_{-N+1} \ \ldots\ J_{N}|$$

$$\underset{\approx}{\psi} = \text{diag}\,|1/\psi_1,\ 1/\psi_2 \ \ldots\ 1/\psi_K|$$

$$\underset{\approx}{T} = \left\| T_{\ell j} \right\| \begin{matrix} \ell = 1, 2, \ldots 2N+1 \\ j = 1, 2, \ldots 2N+1 \end{matrix}$$

$$\underset{\approx}{B} = \left\| B_{\ell i} \right\| \begin{matrix} i = 1, 2, \ldots K \\ \ell = 1, 2, \ldots 2N+1 \end{matrix}$$

The elements of $\underset{\approx}{B}$ and $\underset{\approx}{T}$ are defined by (15) and (16) respectively, and the actual indices are related to the previous ones by $\ell = p + N + 1$, $j = n + N + 1$.

The linear system defined by (17) can be written in terms of these matrices if we neglect the contribution of modes with order greater than N, this assumption implying the truncation of the infinite series down to 2N+1 terms. This procedure allows the determination of the mode coefficient vector as

$$\underset{\sim}{m} = \frac{j}{2\pi Y_e} \left(\underset{\approx}{F} - \frac{\varepsilon_2 k_1 R_1}{\pi \varepsilon_1} \underset{\approx}{J}\ \underset{\approx}{T}\ \underset{\approx}{\Lambda} \right)^{-1} \underset{\approx}{B}\ \underset{\sim}{\xi} \tag{21}$$

Voltages and currents at the i-th disk reference plane are given by

$$V_{di} = - \frac{h}{2\psi_i} \int_{\gamma_i} E_2^{(1)}\ (R_1, \phi)\ d\phi \tag{22}$$

$$I_{di} = - 4R_1 \psi_i\ H_i \tag{23}$$

hence

$$\underset{\sim}{v}_d = -\frac{h}{2}\,\underset{\approx}{\Psi}\,\underset{\approx}{B}^{+}\,\underset{\approx}{J}\,\underset{\sim}{m}$$

$$\underset{\sim}{\xi} = -\frac{1}{4R_1}\,\underset{\approx}{\Psi}\,\underset{\sim}{i}_d \qquad (25)$$

By substituting (25) in (21) and the result in (24), the impedance matrix at the disk ports is obtained as

$$\underset{\approx}{Z}_d = jZ_o\,\underset{\approx}{\Psi}\,\underset{\approx}{B}^{+}\,\underset{\approx}{J}\left(\underset{\approx}{F} - \frac{\varepsilon_2 K_1 R_1}{\pi\varepsilon_1}\,\underset{\approx}{J}\,\underset{\approx}{T}\,\underset{\approx}{\Lambda}\right)^{-1}\,\underset{\approx}{B}\,\underset{\approx}{\Psi} \qquad (26)$$

where

$$Z_o = \frac{h}{16\pi R_1}\left(\mu_1/\varepsilon_1\right)^{1/2}$$

We point out that the matrices containing the information about the number of ports, their positions and coupling angles,are completely frequency independent. This lends to (26) a great flexibility, which is useful for design purposes.

Describing the matching networks by their transfer parameters (Fig. 8), we readily obtain the impedance matrix at the K-port reference planes as

$$\underset{\approx}{Z} = \left(\underset{\approx}{\tau}_{11}\,\underset{\approx}{Z}_d + \underset{\approx}{\tau}_{12}\right)\left(\underset{\approx}{\tau}_{21}\,\underset{\approx}{Z}_d + \underset{\approx}{\tau}_{22}\right)^{-1} \qquad (27)$$

where

$$\underset{\approx}{\tau}_{ij} = \mathrm{diag}\left[\tau_{ij1}, \tau_{ij2}, \cdots, \tau_{ijk}\right] \qquad i,j = 1,2$$

VI. CLASSICAL RESULTS

The classical expression for the input admittance of the three port circulator is derived using the fact that the input impedance of an ideal circulator [10] is given by

$$Z_{in} = Z_{11} - Z_{12}^2/Z_{13} \tag{28}$$

In order to arrive at the results existing in the literature [11], which were derived neglecting the fringing fields, we compute (26) retaining only the modes $n = \pm 1$, and neglecting the fringing function.

After some manipulations, we obtain

$$\underset{\approx}{Z}_d = j\, Z_o \left(\frac{2\sin\psi}{\psi}\right) \; J_1(k_1R_1) \begin{bmatrix} z_1 & z_2 & z_3 \\ z_3 & z_1 & z_2 \\ z_2 & z_3 & z_1 \end{bmatrix} \tag{29}$$

where

$$z_1 = 1/F_1 - 1/F_{-1}$$

$$z_2 = \exp(j2\pi/3)/F_1 - \exp(-j2\pi/3)/F_{-1}$$

$$z_3 = z_2^*$$

With the help of (29) and (28) we obtain for the input admittance

$$Y_{in} = (3Z_o)\left(\frac{\psi}{2\sin\psi}\right)^2 \left[\sqrt{3}\,\frac{\kappa/\mu}{k_1R_1} - j\,\frac{J_1'(k_1R_1)}{J_1(k_1R_1)}\right] \tag{30}$$

Expanding the Bessel functions around $k_1R_1 = 1.84$ it is possible to compare (30) to the input admittance of a shunt loaded resonator near its center frequency ω_o [11]

$$Y = G(1 + j2\delta Q_L) \tag{31}$$

where

$$\delta = (\omega - \omega_o)/\omega_o$$

and Q_L is the loaded Q of the circuit.

Matching (30) to (31) we obtain

$$G = \frac{4\pi}{\sqrt{3}} \frac{R_1}{h} \frac{\sqrt{\varepsilon_1}}{\sqrt{\mu_1}} \left(\frac{\psi}{\sin\psi}\right)^2 \left|\frac{\kappa}{\mu}\right| \tag{32}$$

$$Q_L = 0.69 \left|\kappa/\mu\right|^{-1} \tag{33}$$

Equations (32) and (33) coincide with the revised treatment of Fay-Comstock [2] given by von Aulock-Fay [11]. It is interesting to remark that their results were obtained through an independent method based on the stored energy in the cavity. The only missing term in their expression is $(\psi/\sin\psi)^2$ since the actual coupling to the lines was not considered.

VII. CIRCULATOR SYNTHESIS

In this section a numerical method for the synthesis of a K-port circulator in a symmetrical cavity is presented.

The first step is to determine the scattering matrix at the disk reference planes with the help of (26). The normalization impedance at these planes must be taken as the ideal circulating impedance,

$$\bar{Z}_c = Z^*_{in}$$

where Z_{in} is given by (28). In order to obtain the circulation locus in the plane $(k_1R_1, \kappa/\mu)$ we must find the points where s_{11} , s_{31} , ..., s_{K1} are essentially zero.

The next step is to synthesize the matching networks which transform the circulating impedance into the reference impedance at the K-port planes. The impedance matrix can then be computed from (27) and the overall behavior can be numerically optimized. In order to illustrate the above procedure the circulation locus for a 4-port junction was determined (Fig. 9). On the same figure, we also show the locus computed neglecting the fringing fields. A comparison of the two loci shows a shift in the circulation frequencies which is of the order of 20%. A remarkable feature of this locus is the existence of a double branch for low values of k_1R_1, which is an ideal condition for the synthesis of a broad band device. Circulation in the upper range was earlier reported [7], [8], but as expected, only within narrow bandwidths.

In order to test the feasibility of broadband performance, a prototype was designed at the center frequency operating parameters

$$k_1 R_1 = 2.1$$

$$\kappa/\mu = 0.5$$

The input impedance computed via (28) was transformed to 50 Ω with the aid of two sections of transmission line. Experimental results and prototype parameters are shown in Fig. 10.

VIII. CONCLUSION

A self consistent theory for the analysis of an anisotropic disk n-port, which includes the fringing fields has been developed. Classical results for 3-port circulators are easily derived as a particular case and agree with previously published work. Applicability to numerical design is exemplified with the synthesis of a broad band 4-port circulator. Based on the results when compared with those provided by the magnetic wall assumption, we believe that the inclusion of the fringing fields has resulted in a more accurate theory.

APPENDIX

The symmetry of the structure, together with Maxwell's equations and separation of variables leads to the following form for the fields in both regions

$$\underset{\sim}{E}^{(i)}(r,\phi,z) = \underset{\sim}{E}_t^{(i)}(r,\phi)\ \sin\beta_i z + E_{zt}^{(i)}(r,\phi)\ \cos\beta_i z\ \tilde{z} \qquad (A.1)$$

$$\underset{\sim}{H}^{(i)}(r,\phi,z) = \underset{\sim}{H}_t^{(i)}(r,\phi)\ \cos\beta_i z \qquad (i = 1, 2) \qquad (A.2)$$

where $\underset{\sim}{E}_t$ and $\underset{\sim}{H}_t$ are parallel to the ground plane. Only the modes without r.f. magnetic field in the z direction are being considered.

Substitution of (A.1) and (A.2) into Maxwell's equations leads to Helmoltz's homogeneous equation for E_{zt}

$$(\nabla^2 + k_i^2)\ E_{zt}^{(i)}(r,\phi) = 0 \qquad (A.3)$$

with

$$k_i^2 = \omega^2 \mu_i\ \varepsilon_i - \beta_i^2 \qquad (i = 1, 2) \qquad (A.4)$$

In cylindrical coordinates (A.3) yields the eigenfunctions

$$J_n\ (k_1 r)\ e^{-jn\phi} \qquad \text{for } r \leq R_1$$

$$J_n(k_2 r)\ e^{-jn\phi},\quad Y_n(k_2 r)\ e^{-jn\phi} \qquad \text{for } R_1 \leq r \leq R_2$$

The depth wave number β_i, determined by the boundary conditions

$$\underset{\sim}{E}^{(1)}(r,\phi,h)\times \hat{z} = \underset{\sim}{E}^{(2)}(r,\phi,2h+t)\times \hat{z} = 0$$

are

$$\beta_{1m} = m\pi/h \qquad (A.5)$$

$$\beta_{2m} = m\pi/(2h+t) \qquad m = 0, \pm 1, \pm 2, \ldots \qquad (A.6)$$

The integer m defines the order of the depth mode. The cut-off frequency ω_{im} of the m-th depth mode in region i is, from (A.4),

$$\omega_{im} = \beta_{im}\,(\mu_i\varepsilon_i)^{-1/2}$$

The sign of k_1 and k_2 for the modes below cut-off must be chosen so that the respective eigenfunctions correspond to a decaying field in the radial direction (inwards in medium 1 and outwards in medium 2). This condition leads to the choice of

$$k_i = -j(\beta_i^2 - \omega^2\mu_i\varepsilon_i)^{1/2} \quad \text{when} \quad \omega < \beta_i(\mu_i\varepsilon_i)^{-1/2}$$

The knowledge of the E_{zt} function allows the determination of the field components through the application of Maxwell's equations to (A.1) and (A.2). The eigenfunctions of the zero-th order depth mode of region 1 were determined in [1] and are displayed in Section I of this work. For the outer region we obtain

$$E_{rnm}^{(2)} = \beta_{2m}\,k_2^{-2}\,\frac{\partial E_{zt}^{(2)}}{\partial r}\,\sin\beta_{2m}z$$

$$E^{(2)}_{\phi nm} = \beta_{2m}\, k_2^{-2}\, \frac{\partial E^{(2)}_{zt}}{r\phi\partial}\, \sin\beta_{2m} z$$

$$H^{(2)}_{rnm} = -j\omega\varepsilon_2\ \ (\beta_{2m}\tan\beta_{2m} z)^{-1}\ E^{(2)}_{\phi nm}$$

$$H^{(2)}_{\phi nm} = j\omega\varepsilon_2\ (\beta_{2m}\tan\beta_{2m} z)^{-1}\ E^{(2)}_{rnm}$$

where the $E^{(2)}_{zt}(r,\phi)$ are chosen as

$$E^{(2)}_{zt}(r,\phi) = \left[J_n(k_2 r) - \frac{J_n(k_2 R_2)}{Y_n(k_2 R_2)}\, Y_n(k_2 r)\right] e^{-jn\phi}$$

in order to satisfy the boundary condition

$$E^{(2)}_{z}(R_2,\phi,z) = E^{(2)}_{\phi}(R_2,\phi,z) = 0$$

When the radial wave number k_2 is imaginary, it is more convenient for numerical purposes, to compute the special Bessel functions instead of Bessel functions of imaginary argument. Therefore, for the modes below cut-off we have

$$E^{(2)}_{zt}(r,\phi) = \left[\, K_n(j\ k_2\ r) - \frac{K_n(j\ k_2\ R_2)}{I_n(j\ k_2\ R_2)}\, I_n(j\ k_2\ r)\right] e^{-jn\phi}$$

ACKNOWLEDGEMENT

The authors wish to thank Mr. T. Yoneyama for the numerical computations for Fig. 9 and Mr. Paulo R. Tavares for the etching of the stripline circuitry.

REFERENCES

[1] H. Bosma, "On stripline Y-circulation at UHF", *IEEE Trans. Microwave Theory Tech.*, vol. MTT-12, pp. 61-72, Jan. 1964.

[2] C. E. Fay and R. L. Comstock, "Operation of the ferrite junction circulator", *IEEE Trans. Microwave Theory Tech.*, vol. MTT-13, pp. 15-27, Jan. 1965.

[3] P. P. Civalleri and S. Ridella, "Impedance and admittance matrices of distributed rectangular structures", *IEEE Trans. Circuit Theory*, vol. CT-A, pp. 392-398, Aug. 1970.

[4] T. Okoshi and T. Miyoshi, "The planar circuit - An approach to microwave integrated circuitry", *IEEE Trans. Microwave Theory Tech.*, vol. MTT-20, pp. 245-252, Apr. 1972.

[5] P. Silvester, "Finite Element Analysis of Planar Microwave Networks", *IEEE Trans. Microwave Theory Tech.*, vol. MTT-21, pp. 104-108, Feb. 1973.

[6] Y. S. Wu and F. J. Rosenbaum, "Wide-band operation of Microstrip Circulators", *IEEE Trans. Microwave Theory Tech.*, vol. MTT-22, pp. 849-856, Oct. 1974.

[7] J. Helszajn, "Waveguide and strip-line 4-port single junction circulators", *IEEE Trans. Microwave Theory Tech.*, vol. MTT-21, pp. 630-633, Oct. 1973.

[8] A. M. Hussein, M. M. Ibrahim and S. E. Youssef, "Performance Characteristics of 4-port Stripline Circulators", *IEEE Trans. Microwave Theory Tech.*, vol. MTT-23, pp. 923-926, Nov. 1975.

[9] K. Tanabe, Y. Kobayashi, and S. Tanaka, "Numerical Analysis of Eigenvalue Solution of Disk Resonator", *IEEE Trans. Microwave Tech.*, vol. MTT-23, pp. 508-511, Jun. 1975.

[10] H. Bosma, "Junction Circulators", In: *Advances in Microwave*, vol. 6, L. Young Ed., New York, Academic Press, 1971.

[11] W. H. von Aulock and C. E. Fay, "Linear Ferrite Devices for Microwave Applications", In: *Advances in Electronic and Electron Physics*, vol. 5, L. Marton Ed., New York, Academic Press, 1968.

[12] D. Polder, "On the theory of ferromagnetic resonance", *Phil. Mag.*, vol. 40, pp. 99-115, Jan. 1949.

FIGURE CAPTIONS

Fig. 1 - Schematic of general 4-port network, launchers and top cover removed.

Fig. 2 - Cross section of cavity.

Fig. 3 - Conductor disk geometry and reference planes.

Fig. 4 - Behaviour of the z component of electric field at the disk edge (first depth mode only).

Fig. 5 - Variation of fringing functions up to second order with normalized frequency and normalized radius as parameter.

Fig. 6 - Variation of fringing function of first order with normalized radius, and normalized frequency as parameter.

Fig. 7 - General behaviour of first resonances of mode $\pm n$ (—— magnetic wall [1], --- Eq. (20), $J'(x_n) = 0$).

Fig. 8 - Transmission parameters of the matching network at i-th port.

Fig. 9 - Circulation locus of symmetric 4-port anisotropic networks (—— magnetic wall assumption, --- fringing fields included, for $\bar{R}_1 = 3.5$, $\bar{R}_2 = 15.$).

Fig. 10 - Experimental results obtained with prototype 4-port circulator.

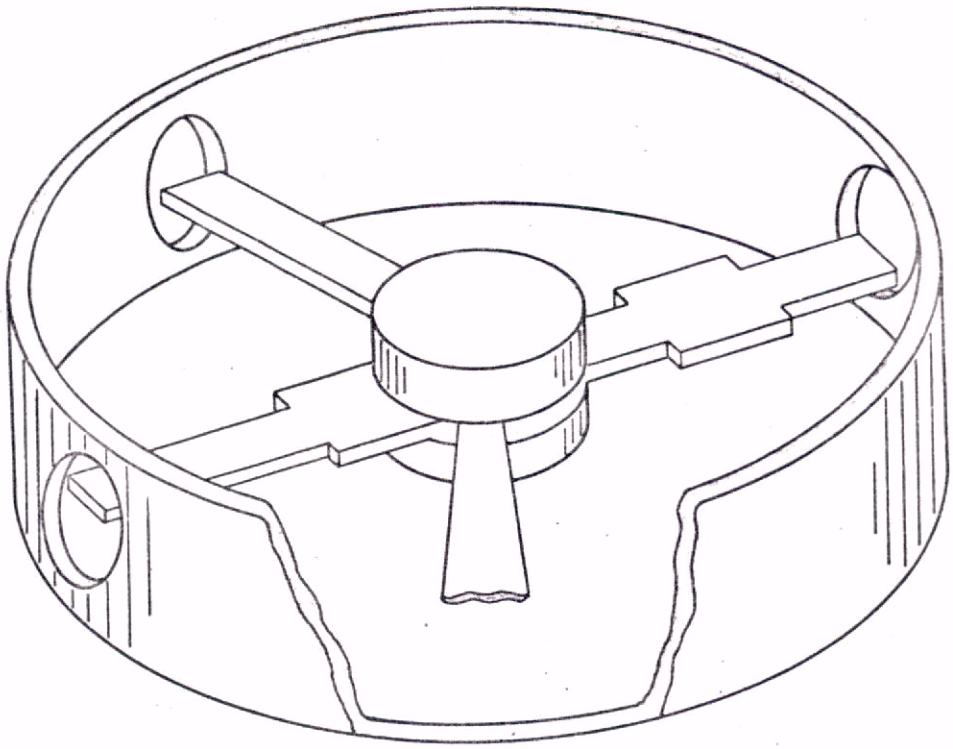

Figure 1

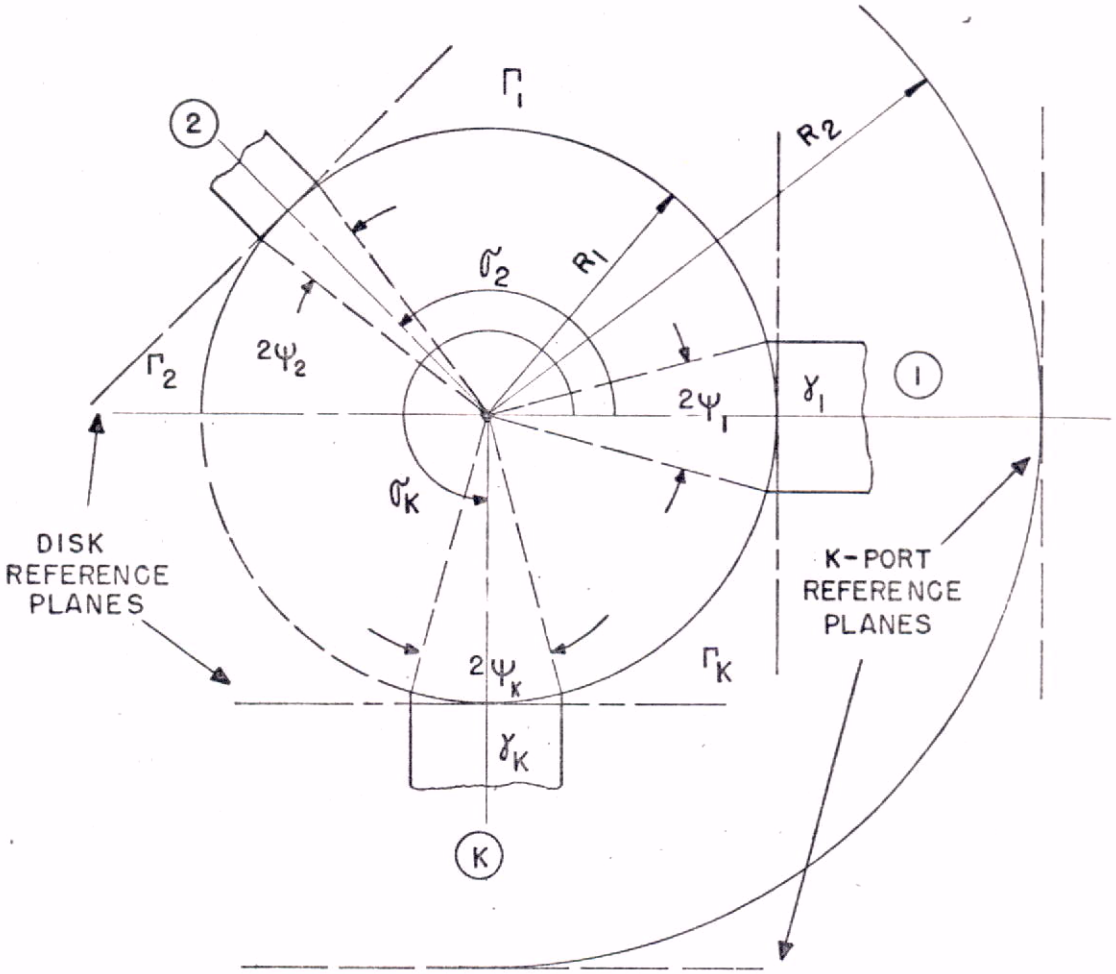
Γ1
2
R2
R1
σ2
2ψ2
Γ2
2ψ1
γ1
1
σK
DISK
REFERENCE
PLANES
K-PORT
REFERENCE
PLANES
2ψK
ΓK
γK
K

Figure 3

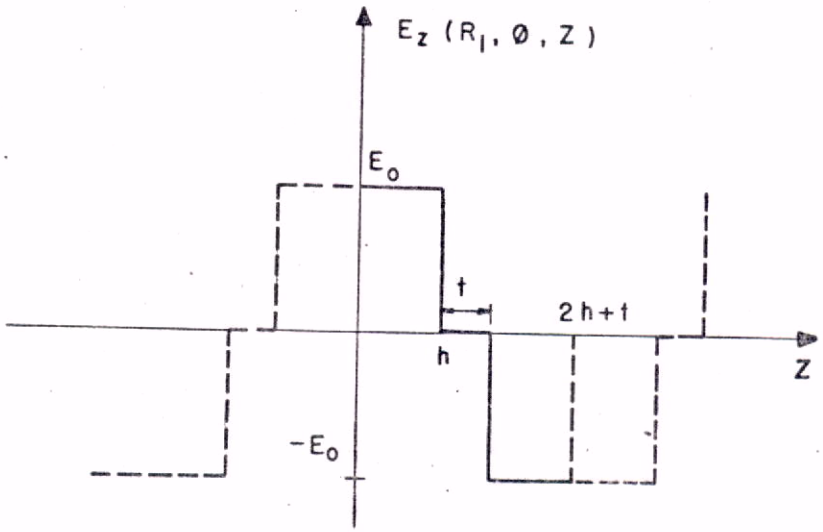

Figure 4

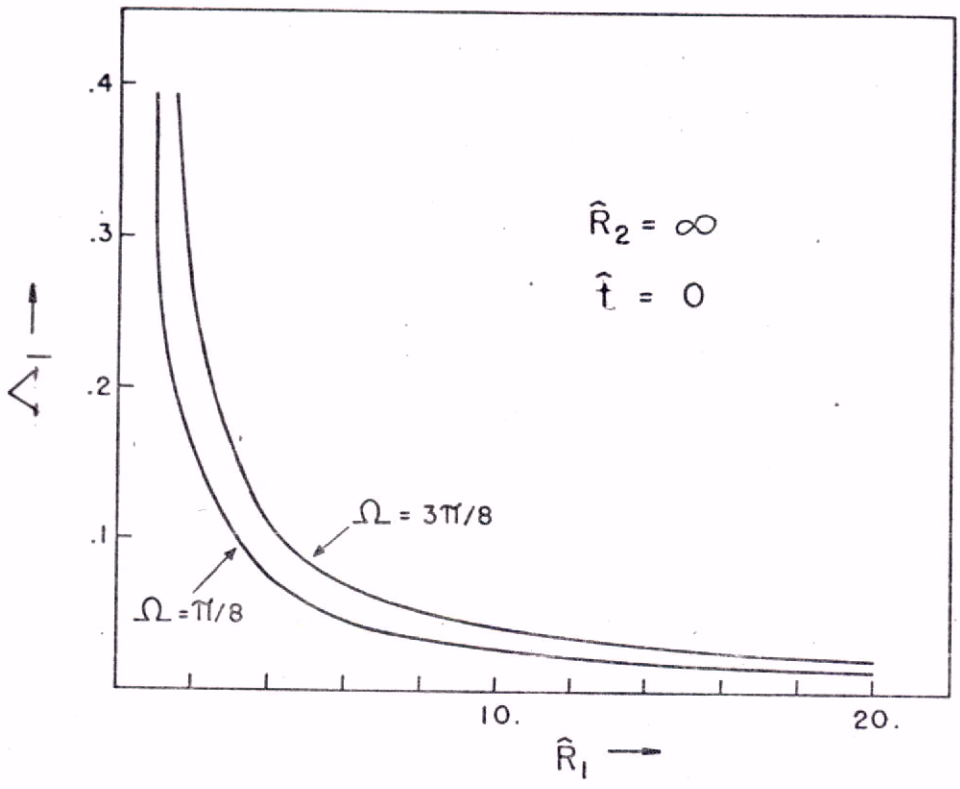

Figure 6

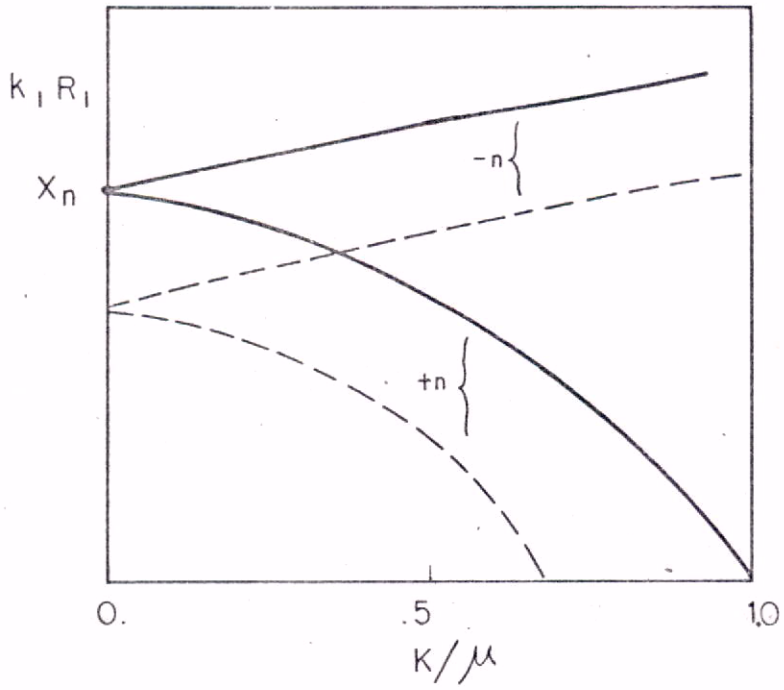

Figure 7

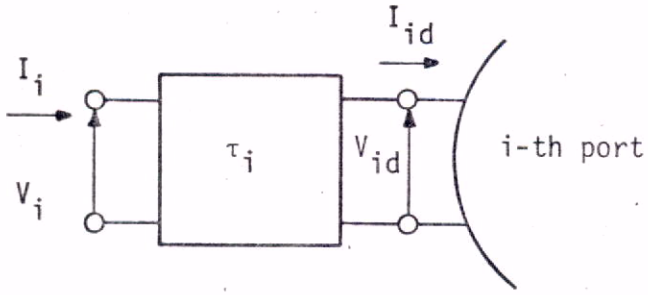

$$V_i = \tau_{11i}\, V_{id} + \tau_{12i}\, I_{id}$$

$$I_i = \tau_{21i}\, V_{id} + \tau_{22i}\, I_{id}$$

Figure 8

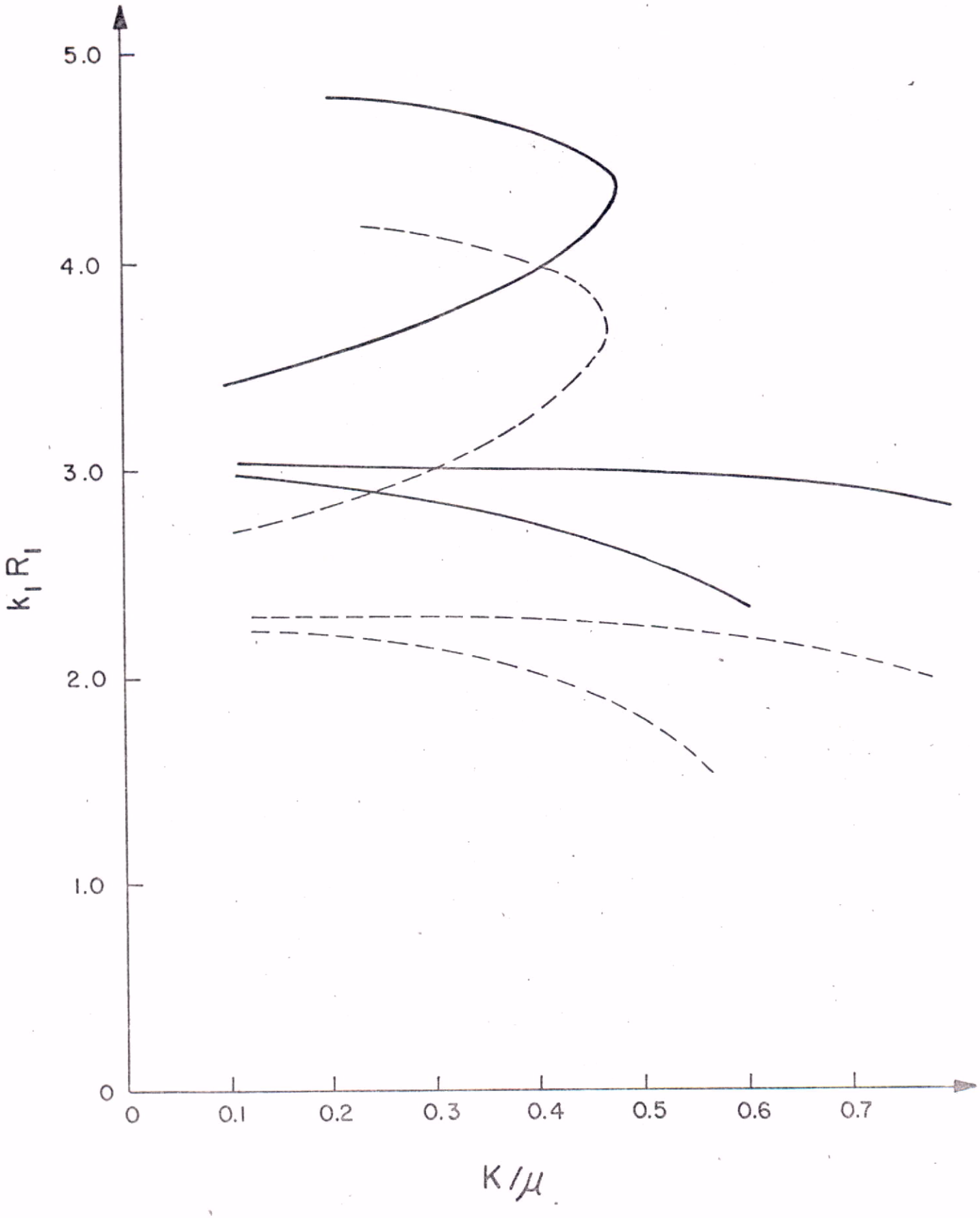

Figure 9

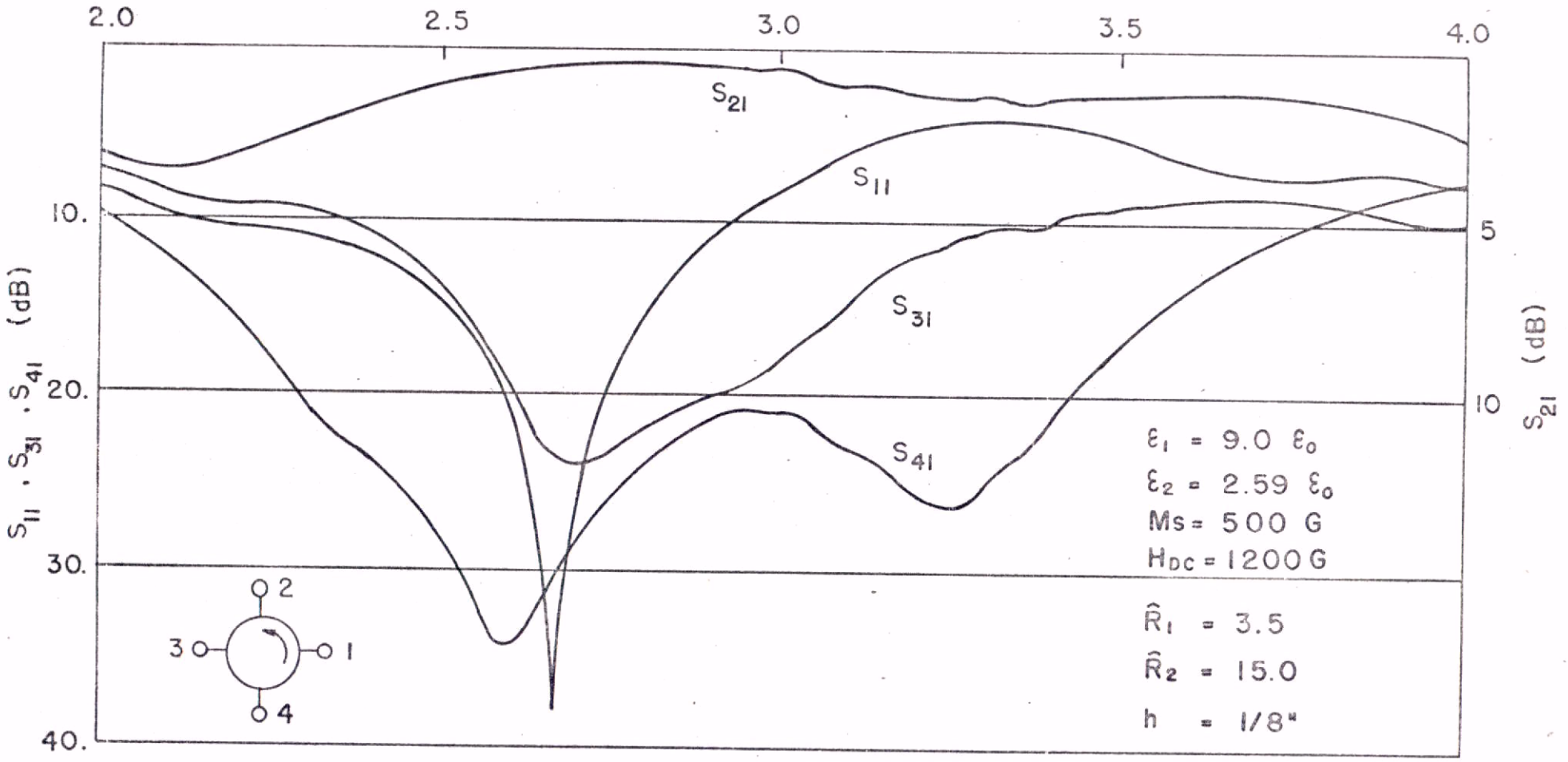
FREQUENCY (GHz)
2.0
2.5
3.0
3.5
4.0
S_{21}
S_{11}
S_{31}
S_{41}
10.
20.
30.
40.
S_{11} , S_{31} , S_{41} (dB)
5
10
S_{21} (dB)
$\varepsilon_1 = 9.0\ \varepsilon_o$
$\varepsilon_2 = 2.59\ \varepsilon_o$
Ms = 500 G
H_{DC} = 1200 G
$\hat{R}_1 = 3.5$
$\hat{R}_2 = 15.0$
h = 1/8"
1
2
3
4

Figure 10